

RESEARCH BRIEF

Isocitrate Dehydrogenase Mutations Confer Dasatinib Hypersensitivity and SRC Dependence in Intrahepatic Cholangiocarcinoma

Supriya K. Saha¹, John D. Gordan², Benjamin P. Kleinstiver^{3,4}, Phuong Vu¹, Mortada S. Najem¹, Jia-Chi Yeo¹, Lei Shi¹, Yasutaka Kato¹, Rebecca S. Levin⁵, James T. Webber², Leah J. Damon¹, Regina K. Egan¹, Patricia Greninger¹, Ultan McDermott⁶, Mathew J. Garnett⁶, Roger L. Jenkins⁷, Kimberly M. Rieger-Christ⁸, Travis B. Sullivan⁸, Aram F. Hezel⁹, Andrew S. Liss¹⁰, Yusuke Mizukami^{1,11}, Lipika Goyal¹, Cristina R. Ferrone¹, Andrew X. Zhu¹, J. Keith Joung^{3,4}, Kevan M. Shokat^{5,12}, Cyril H. Benes¹, and Nabeel Bardeesy¹

ABSTRACT

Intrahepatic cholangiocarcinoma (ICC) is an aggressive liver bile duct malignancy exhibiting frequent isocitrate dehydrogenase (*IDH1*/*IDH2*) mutations. Through a high-throughput drug screen of a large panel of cancer cell lines, including 17 biliary tract cancers, we found that *IDH* mutant (*IDHm*) ICC cells demonstrate a striking response to the multikinase inhibitor dasatinib, with the highest sensitivity among 682 solid tumor cell lines. Using unbiased proteomics to capture the activated kinase and CRISPR/Cas9-based genome editing to introduce dasatinib-resistant “gatekeeper” mutant kinases, we identified SRC as a critical dasatinib target in *IDHm* ICC. Importantly, dasatinib-treated *IDHm* xenografts exhibited pronounced apoptosis and tumor regression. Our results show that *IDHm* ICC cells have a unique dependency on SRC and suggest that dasatinib may have therapeutic benefit against *IDHm* ICC. Moreover, these proteomic and genome-editing strategies provide a systematic and broadly applicable approach to define targets of kinase inhibitors underlying drug responsiveness.

SIGNIFICANCE: *IDH* mutations define a distinct subtype of ICC, a malignancy that is largely refractory to current therapies. Our work demonstrates that *IDHm* ICC cells are hypersensitive to dasatinib and critically dependent on SRC activity for survival and proliferation, pointing to new therapeutic strategies against these cancers. *Cancer Discov*; 6(7); 727–39. ©2016 AACR.

¹Massachusetts General Hospital Cancer Center, Harvard Medical School, Boston, Massachusetts. ²Helen Diller Family Comprehensive Cancer Center, University of California, San Francisco, San Francisco, California. ³Molecular Pathology Unit, Center for Cancer Research, and Center for Computational and Integrative Biology, Massachusetts General Hospital, Charlestown, Massachusetts. ⁴Department of Pathology, Harvard Medical School, Boston, Massachusetts. ⁵Department of Cellular and Molecular Pharmacology, University of California, San Francisco, San Francisco, California. ⁶Wellcome Trust Sanger Institute, Hinxton, UK. ⁷Department of Transplantation, Lahey Hospital and Medical Center, Burlington, Massachusetts. ⁸Department of Translational Research, Lahey Hospital and Medical Center, Burlington, Massachusetts. ⁹University of Rochester School of Medicine, Rochester, New York. ¹⁰Department of Surgery and the Andrew L. Warshaw, MD, Institute for Pancreatic Cancer Research, Massachusetts General Hospital and Harvard Medical School, Boston, Massachusetts. ¹¹Center for Clinical and Biomedical Research, Sapporo

Higashi Tokushukai Hospital, Sapporo, Hokkaido, Japan. ¹²Howard Hughes Medical Institute, University of California, San Francisco, San Francisco, California.

Note: Supplementary data for this article are available at *Cancer Discovery* Online (<http://cancerdiscovery.aacrjournals.org/>).

Corresponding Authors: Nabeel Bardeesy, Massachusetts General Hospital, 185 Cambridge Street, CPZN 4216, Boston, MA 02114. Phone: 617-643-2579; Fax: 617-643-3170; E-mail: nabardeesy@partners.org; and Cyril H. Benes, CNY 149 Room 7401, 149 13th Street, Charlestown, MA 02129. Phone: 617-724-3409, Fax: 617-726-7808; E-mail: cbenes@mgh.harvard.edu

doi: 10.1158/2159-8290.CD-15-1442

©2016 American Association for Cancer Research.

INTRODUCTION

Biliary tract cancers (BTC) include a spectrum of invasive adenocarcinomas encompassing both cholangiocarcinoma arising in the intrahepatic, perihilar, or distal biliary tree, and carcinoma arising from the gallbladder (1). As a subset of BTCs, intrahepatic cholangiocarcinoma (ICC) is the second most common type of primary liver tumor, and has been rising in incidence worldwide for the past three decades (2). The reported incidence of ICC in the United States has risen from 0.44 per 100,000 in 1973 to 1.18 in 2012 (3), although the actual rate is likely significantly higher, as recent molecular studies demonstrate that “carcinomas of unknown primary” are most commonly biliary in origin (4, 5). Despite the current standard chemotherapy with gemcitabine/cisplatin combination for patients with unresectable or metastatic BTCs, the median survival time remains less than 1 year (6), and there are no standard treatments for patients after progression on this regimen.

Recent work has provided a detailed view of the genetics of ICC (7–14), revealing that specific gain-of-function hotspot mutations in isocitrate dehydrogenase 1 and 2 (*IDH1/IDH2*) are among the most common genetic lesions in ICC (present in ~18%–37% of ICC cases in North America and Europe). These mutations occur within the isocitrate binding site of IDH1 (R132) or IDH2 (R172, R140) and cause altered enzymatic function, leading to the production of *R*(-)2-hydroxyglutarate (2-HG), a proposed “oncometabolite” (15). 2-HG inhibits members of the family of α -ketoglutarate-dependent dioxygenase enzymes, many of which function as epigenetic modifiers, resulting in genome-wide changes in the landscape of DNA and histone methylation marks (16–18). Mutant IDH impairs differentiation of a number of cell lineages in a 2-HG-dependent manner. In the mouse liver, mutant IDH blocks adult liver progenitor cells from undergoing hepatocyte differentiation as an early event in ICC pathogenesis (19, 20). Accordingly, the IDH mutant (IDHm) subset of ICC has a distinct transcriptional signature compared to IDH wild-type (WT) tumors, characterized by enrichment of hepatic stem cell genes (19, 20).

There is a great deal of interest in the pharmacologic targeting of the mutant IDH enzyme and evidence of highly significant responses in patients with acute myeloid leukemia treated with an IDH2 inhibitor (21). In advanced ICC, the role for mutant IDH remains unclear. Recently reported results from the ongoing phase I study of AG-120, the first-in-class IDH1 inhibitor, have demonstrated the potential for IDH inhibition to promote transient stabilization of disease in a subset of patients with IDHm ICC (22); however, alternative or combinatorial strategies may be needed for durable remissions. Beyond inhibition of the mutant IDH enzyme, we hypothesized that the widespread changes in cell differentiation state, cell metabolism, and epigenetic control provoked by *IDH* mutations (15) may confer additional vulnerabilities that can be targeted (23). We utilized a large-scale high-throughput drug screen to uncover such synthetic lethal therapeutic interactions. Our results reveal that IDHm ICC represents a distinct subtype of ICC with a unique molecular signature and drug response profile. Most significantly, this approach revealed that IDHm cells were highly responsive to dasatinib,

exhibiting the greatest sensitivity to this drug among all 682 solid tumor cell lines tested, which we demonstrated was due to a critical dependency on SRC signaling. Importantly, this potency corresponded to levels and duration of exposure that are readily attainable in the clinic, and, accordingly, dasatinib caused rapid and widespread cell death in IDHm patient-derived xenografts (PDX). Thus, we have identified a novel and dramatic therapeutic vulnerability conferred by mutant IDH in ICC that has immediate translational potential.

RESULTS

We assembled a collection of 17 BTC cell lines representing ICC, extrahepatic cholangiocarcinoma (ECC), and gallbladder cancer (GBC). Sequencing analysis identified two ICC cell lines with *IDH1* mutations: RBE (R132S) and SNU-1079 (R132C). Neither cell line demonstrated specific sensitivity to the mutant IDH1 inhibitor AGI-5027, compared with *IDH* WT ICC cell lines under normal *in vitro* growth conditions, despite effective reduction in 2-HG levels (Supplementary Fig. S1A–B). In order to identify alternative therapeutic strategies in this ICC subset, we subjected our BTC cell line collection to a high-throughput drug screen with 122 FDA-approved drugs or other clinically relevant compounds (Fig. 1A; Supplementary Table S1). By quantifying the relative response to compounds targeting a wide range of pathways, this screen also allows us to generate a unique and functionally relevant drug-sensitivity profile for each BTC cell line.

A broad range of responses to the different agents was observed across the cell line collection, with specific activity profiles for different BTC subtypes (Fig. 1B; Supplementary Table S1). Notably, the two IDHm ICC cell lines segregated together in unbiased clustering analysis and apart from all the other BTC cell lines in the screen (Fig. 1B and Supplementary Fig. S2). Across the panel of drugs screened, the IDHm ICC lines were marked outliers in their response to the multi-tyrosine kinase inhibitor (TKI) dasatinib (Fig. 1C). Most strikingly, when compared with a larger panel of 684 solid tumor cell lines screened in parallel, the IDHm ICCs ranked first and second in sensitivity (Fig. 1D, *x*-axis: compare red dots and gray dots; Supplementary Table S2). The sensitivity of IDHm ICC was also among the top 8th percentile when compared to 201 hematopoietic cancer cell lines, with the small set of more responsive lines enriched for chronic myelogenous leukemias (CML) harboring BCR-ABL translocations, in keeping with the inhibition of ABL activity by dasatinib and the highly effective clinical use of this drug in the treatment of translocation-positive CML (Fig. 1D; Supplementary Table S2; refs. 24, 25). Both IDHm ICC lines also demonstrated outlier sensitivity to saracatinib, a structurally unrelated TKI with an overlapping target profile (26, 27), suggesting a common mechanism of action (Fig. 1D, *y*-axis; Supplementary Table S2). Thus, IDHm ICC cells show exceptional responsiveness to these inhibitors at a dose range suggesting potential clinical relevance.

We validated these findings in scaled-up proliferation assays across our set of ICC cell lines and included the immortalized human cholangiocyte line MMNK-1 as an additional reference. These studies confirmed that both RBE and SNU-1079 cells were highly sensitive to dasatinib (IC_{50} of 1 nmol/L and

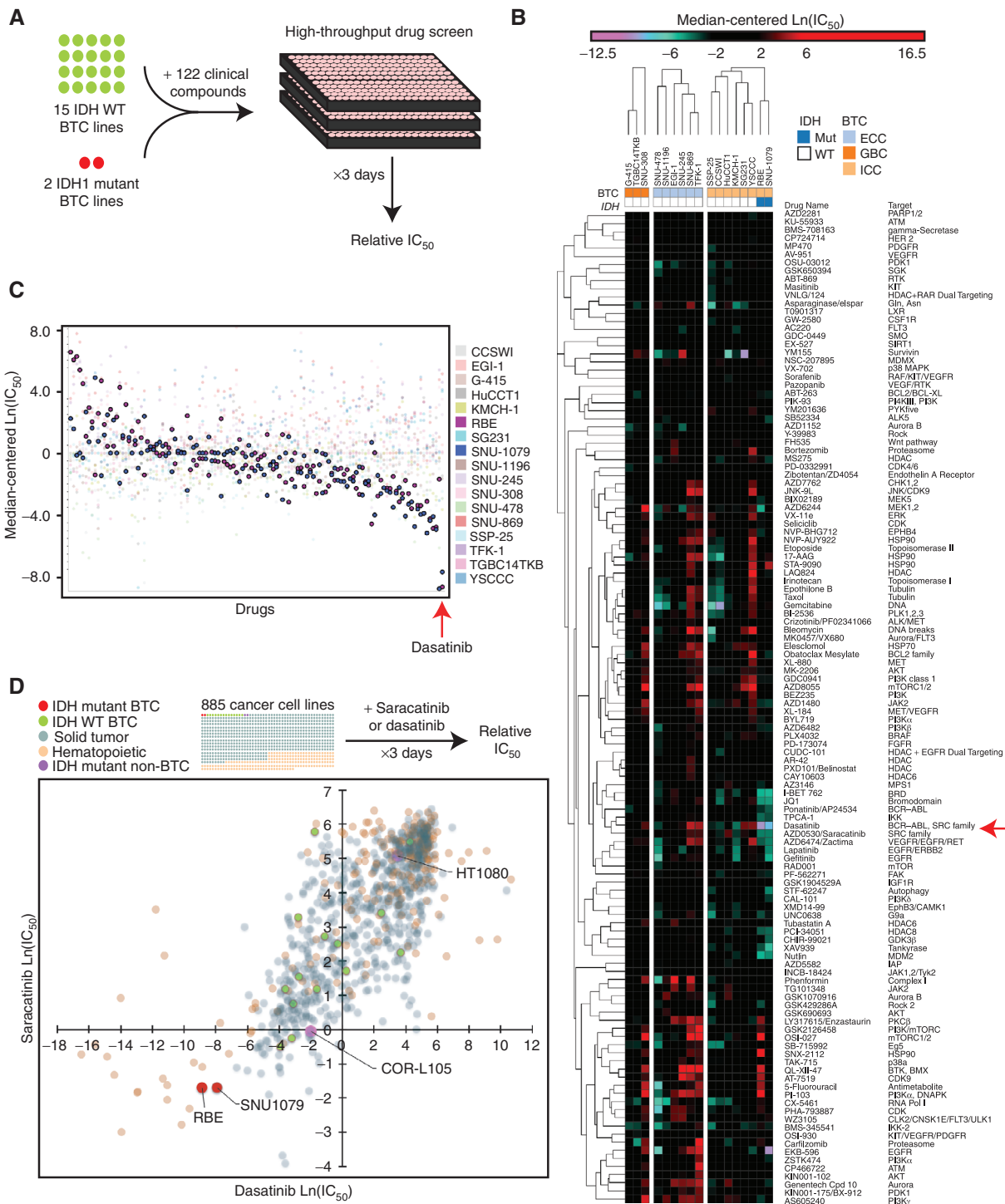


Figure 1. IDHm ICC cells are hypersensitive to dasatinib. **A**, schematic of the high-throughput drug screen protocol. 15 IDH WT BTC and two IDHm ICC cell lines were screened across 122 approved or advanced clinical compounds at nine different doses. Viability was quantified at 72 hours and the IC_{50} estimated for each compound and cell line. **B**, heat map illustrating the median-centered $\ln(\text{Ln}(IC_{50}))$ of 17 BTC cell lines screened across 122 clinically relevant compounds. Note that the two IDHm ICC lines segregate together in unbiased hierarchical clustering. **C**, relative sensitivity [y-axis natural log scale, 0 = median $\ln(\text{Ln}(IC_{50}))$ across all BTC tested] of two IDHm ICC lines to 122 individual drugs (ranked by average sensitivity of IDHm ICC, x-axis). Dasatinib demonstrates the greatest selective activity against IDHm ICC among drugs screened. **D**, sensitivity of 885 cancer cell lines to dasatinib (x-axis) and saracatinib (y-axis), each represented by an individual dot. IDHm ICC lines RBE (IDH1 R132S) and SNU-1079 (IDH1 R132C) are the two larger red dots. IDHm non-BTC cell lines HT1080 (IDH1 R132C) and COR-L105 (IDH1 R132C) are represented by purple dots. Drug response is presented as the natural logarithm of the IC_{50} in $\mu\text{mol/L}$.

7 nmol/L, respectively) compared to a panel of other human ICC cell lines (IC_{50} range, 29–562 nmol/L) and MMNK-1 cells (IC_{50} 776 nmol/L; Fig. 2A, first panel, and Supplementary Table S3). We also confirmed the increased sensitivity of RBE and SNU-1079 cells to saracatinib relative to the IDH WT lines (Fig. 2A). These responses did not reflect a general hypersensitivity to TKIs, because two other multi-TKIs with overlapping but distinct target profiles, bosutinib and ponatinib, were similarly potent against IDH WT and IDHm ICC cell lines (Fig. 2A). To extend these findings, we generated a set of novel low-passage human ICC cell lines from resected tumor specimens, which included an additional line harboring an endogenous *IDH1* R132V mutation (designated ICC5). As with our established cell lines, ICC5 cells were highly and specifically responsive to dasatinib, with an IC_{50} of ~1 nmol/L versus 175 nmol/L and 87 nmol/L in the IDH WT ICC1 and ICC2 lines, respectively (Fig. 2B and Supplementary Table S3). Moreover, ICC5 showed sensitivity profiles that were comparable to our established IDHm ICC lines across each of the other three TKIs, strongly suggesting that dasatinib and saracatinib target a common conserved dependency in this ICC subset (Fig. 2B). Importantly, dasatinib induced rapid cell death specifically in IDHm ICC cell lines, as assessed by crystal violet staining and cleaved caspase-3 activity assays at 24 hours (Supplementary Fig. S3A and S3B). This pronounced sensitivity to dasatinib was not a general feature of IDHm cancers across different tissues, because cell lines derived from IDHm chondrosarcoma or lung adenocarcinoma (HT-1080, SW-1353, and COR-L105) were all relatively resistant when compared to IDHm ICC cells (IC_{50} = 1,578 nmol/L, 120.8 nmol/L, and 43.5 nmol/L, respectively; Supplementary Fig. S3C). Along these lines, IDHm ICC did not show differential sensitivity to agents reported to be selectively toxic to IDHm cancer cells from other tissues, including the BCL2 inhibitor ABT-199 and the nicotinamide phosphoribosyltransferase (NAMPT) inhibitor FK866, which were observed to have enhanced activity against IDHm leukemia and glioma, respectively (Supplementary Fig. S3D and S3E; refs. 28, 29). Thus, our data indicate that dasatinib has potent and specific synthetic lethal interactions with *IDH* mutations in ICC, and that IDHm status is associated with distinct vulnerabilities in different cancer types.

The potency of dasatinib in patients with BCR-ABL-driven CML relates to rapid induction of apoptosis, because this drug has a relatively short serum half-life (~4–6 hours; refs. 24, 25). Thus, we next tested whether brief exposure to physiologically attainable concentrations of dasatinib induces lasting effects on IDHm ICC cells. SNU-1079 and MMNK-1 control cells were exposed to 100 nmol/L dasatinib for 4 hours and then switched to drug-free media for 48 hours. Remarkably, this transient treatment induced profound lethality in IDHm ICC cells, with very few cells remaining after 48 hours (Supplementary Fig. S3F). We then extended our analysis of the correlation between *IDH* status and drug-sensitivity profiles by comparing cell lines derived from genetically engineered mouse models of ICC harboring *IDH2^{R172K}* and *KRAS^{G12D}* mutations (SS49 cells) or *KRAS^{G12D}* mutation and p53 deletion (425 and 537 cells; refs. 20, 30). The IDHm ICC SS49 cells were highly sensitive to dasatinib (IC_{50} = 3.6 nmol/L, vs. > 100 nmol/L in 425 and 537 cells) and, to a lesser extent, saracatinib, whereas the effects of bosutinib and ponatinib

were comparable between genotypes, in line with the effects seen in human ICC cells (Fig. 2C).

SS49 cells form robust tumors upon subcutaneous implantation in SCID mice, enabling us to test the sensitivity of IDHm ICCs *in vivo*. Treatment with dasatinib (50 mg/kg daily) was initiated once tumors reached a volume of ~125 mm³. Notably, dasatinib-treated tumors demonstrated rapid and sustained remission through 2 weeks of treatment (Fig. 2D). Histologic analysis of tumors harvested after 2 days of dasatinib treatment revealed widespread necrotic tissue and activation of the apoptotic marker cleaved caspase-3, whereas vehicle-treated tumors were composed exclusively of viable ductal epithelia and stroma (Fig. 2E). These effects were progressive, because residual tumors harvested after 14 days of treatment exhibited increasing areas of hyalinized and necrotic tissue (Fig. 2E). Finally, we developed a human PDX model (SS110) from a resected ICC harboring an *IDH1* R132C mutation. Tumor fragments were passaged subcutaneously in immunocompromised mice and never adapted to tissue culture conditions. Established SS110 tumors (passage 2) were allowed to reach ~900 mm³ and then treated with dasatinib for 7 days. Similar to our murine xenograft model, these PDX tumors responded by undergoing rapid and widespread necrosis (Fig. 2F). By contrast, dasatinib had only minimal effects on the growth of an IDH WT ICC PDX (Supplementary Fig. S3G and S3H). Thus, IDHm ICC cells demonstrate pronounced sensitivity to clinically relevant doses of dasatinib both *in vitro* and *in vivo*.

To gain insight into the mechanism underlying dasatinib sensitivity, we examined the impact of dasatinib on major oncogenic pathways in IDH WT and mutant ICC cells over a time course of treatment. A series of key signaling networks, including the MAPK pathway (pERK1/2), the JAK-STAT pathway (pSTAT3), and pro/antiapoptotic proteins (BCL2, MCL1, BIM, and PUMA), were all completely unaffected by cytotoxic concentrations of dasatinib over 6 hours of exposure (Fig. 3A; data not shown). By contrast, markers of mTOR complex 1 (mTORC1) activation (p-p70S6K and pS6) were potently inhibited between 1 and 6 hours of treatment exclusively in IDHm cells, suggesting a genotype specificity of pathways downstream of dasatinib-targeted kinases in ICC (Fig. 3A). Correspondingly, inhibition of mTOR with low concentrations of Torin 1 (5–25 nmol/L) effectively reduced p-p70S6K and pS6 levels and slowed cell proliferation of IDHm and IDH WT ICC cells (Supplementary Fig. S4A–B), indicating that mTOR signaling supports the growth of all ICCs, and suggesting that specific control of mTORC1 downstream of dasatinib-targeted kinases contributes to the dasatinib sensitivity of IDHm cells.

We subsequently wished to determine the direct target(s) underlying the effect of dasatinib in IDHm ICC cells among the >40 kinases that are known to be inhibited by this drug at the dose range used in our studies (26, 31). First, we used a multiplexed inhibitor bead (MIB) column strategy in order to generate a comprehensive and unbiased list of active kinases that are inhibited by dasatinib in IDHm ICC cells (32, 33). In this approach, activated kinases in cell lysates are identified through their preferential binding to a column containing 12 kinase inhibitors coupled to sepharose beads. This allows broad capture of active kinases in untreated cells, and

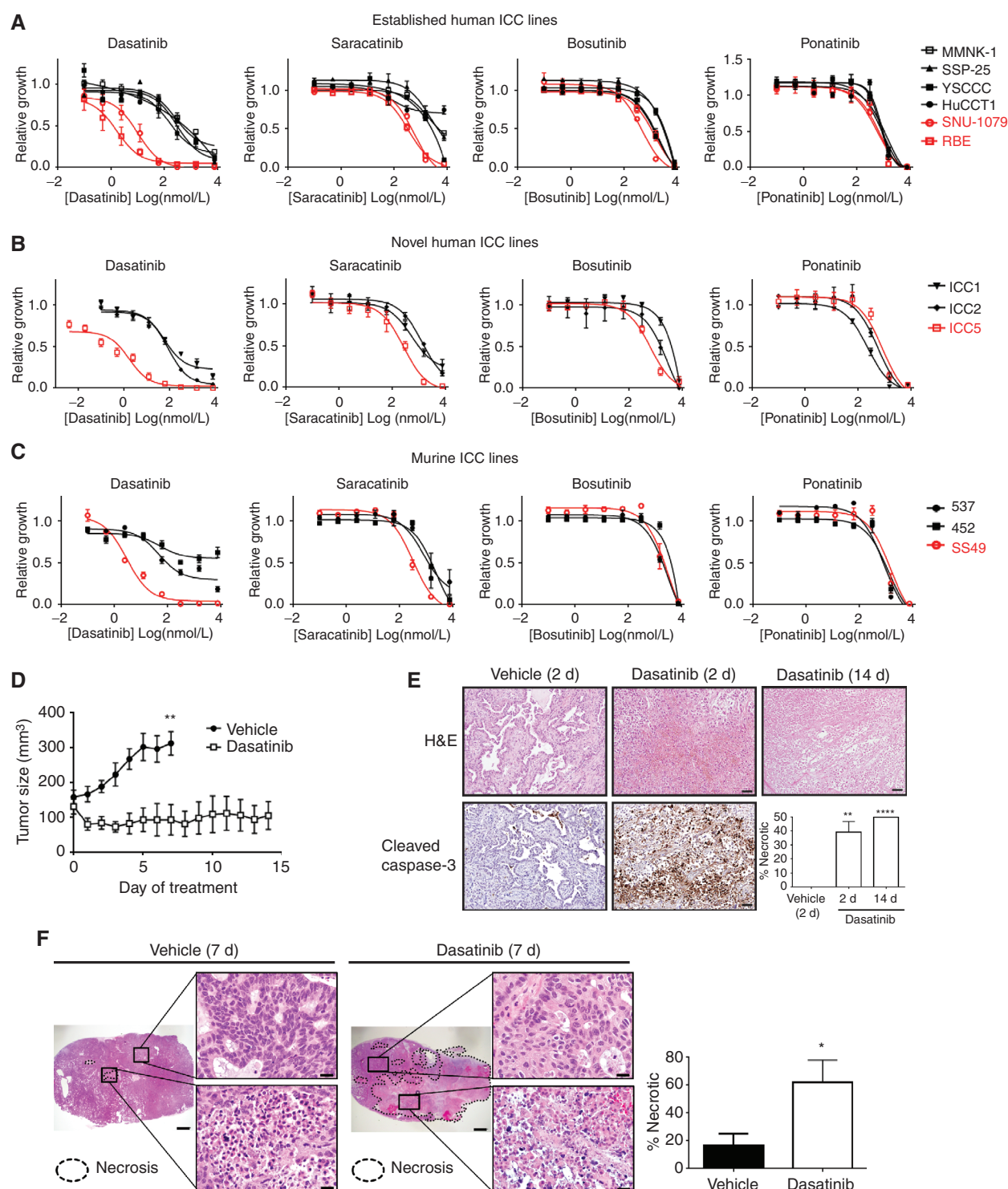


Figure 2. *In vitro* and *in vivo* hypersensitivity of IDHm ICC to dasatinib. **A–C**, proliferation curves of established human (**A**), novel human (**B**), and murine (**C**) IDHm (red) and WT (black) ICC lines and MMNK-1 cells treated with increasing doses of the TKIs dasatinib, saracatinib, bosutinib, and ponatinib. **D** and **E**, tumors arising from subcutaneously implanted murine IDHm ICC (SS49) cells were treated with either vehicle control or dasatinib 50 mg/kg daily by oral gavage. **D**, serial tumor size measurements. **E**, histologic analysis and immunostaining at the indicated time points revealed that dasatinib treatment causes widespread necrosis and activation of apoptotic markers. Top, hematoxylin and eosin (H&E) stain; bottom, immunohistochemistry for cleaved caspase-3; inset: quantification of % necrotic tumor for vehicle ($n = 3$) or dasatinib treatment ($n = 7$ at 2 days, $n = 5$ at 14 days). Scale bars, 50 μm . **F**, histologic analysis (H&E) of an IDH1 R132C ICC PDX treated with vehicle control or dasatinib 50 mg/kg daily by oral gavage for seven days. Right, quantification of the percentage of necrotic tumor for vehicle ($n = 5$) and dasatinib treatment ($n = 5$). Scale bars, 1 mm (low-power images) or 20 μm (high-power images). * $P < 0.05$; ** $P < 0.01$; *** $P < 0.0001$.

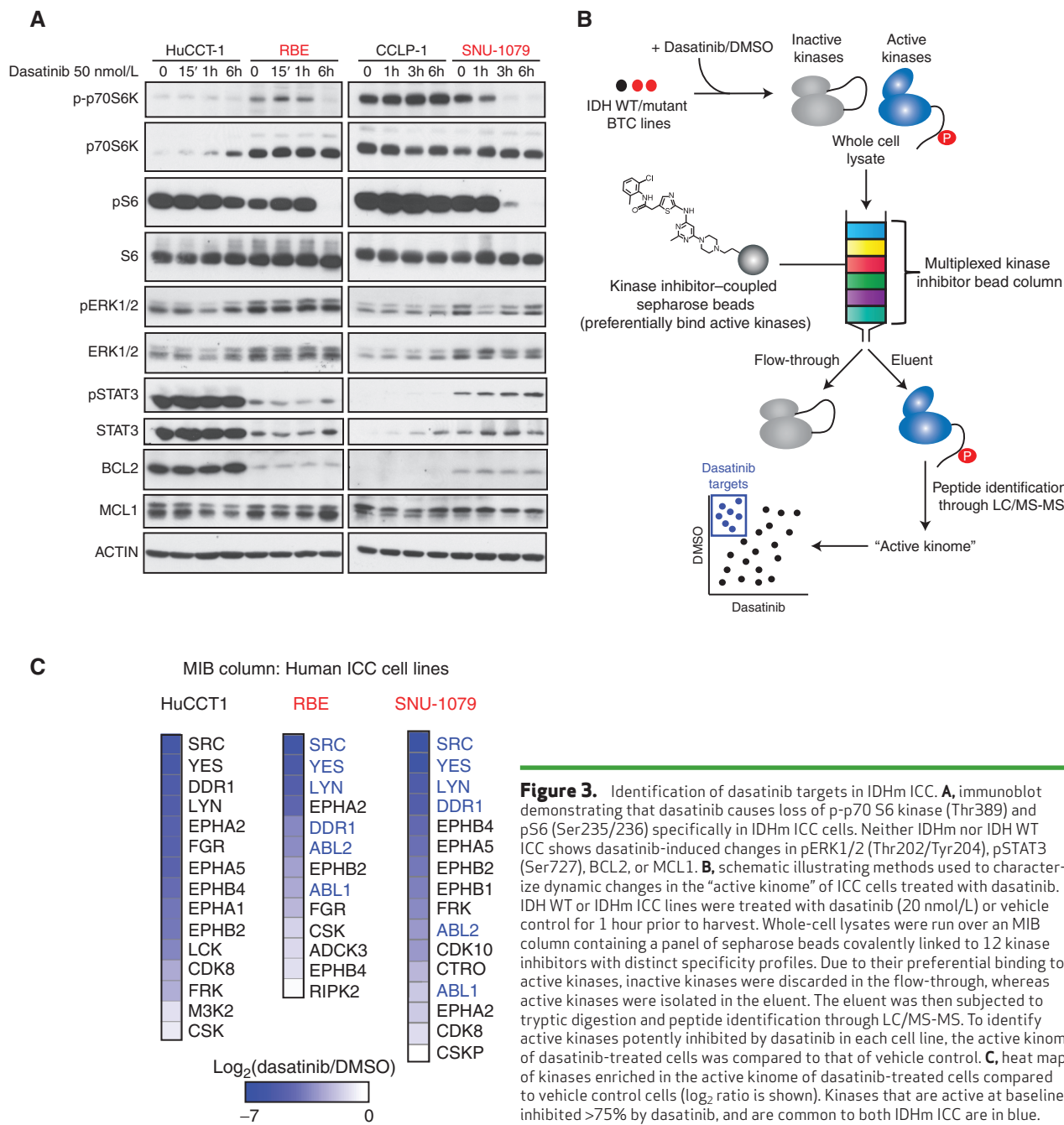


Figure 3. Identification of dasatinib targets in IDHm ICC. **A**, immunoblot demonstrating that dasatinib causes loss of p-p70 S6 kinase (Thr389) and pS6 (Ser235/236) specifically in IDHm ICC cells. Neither IDHm nor IDH WT ICC shows dasatinib-induced changes in pERK1/2 (Thr202/Tyr204), pSTAT3 (Ser727), BCL2, or MCL1. **B**, schematic illustrating methods used to characterize dynamic changes in the "active kinase" of ICC cells treated with dasatinib. IDH WT or IDHm ICC lines were treated with dasatinib (20 nmol/L) or vehicle control for 1 hour prior to harvest. Whole-cell lysates were run over an MIB column containing a panel of sepharose beads covalently linked to 12 kinase inhibitors with distinct specificity profiles. Due to their preferential binding to active kinases, inactive kinases were discarded in the flow-through, whereas active kinases were isolated in the eluent. The eluent was then subjected to tryptic digestion and peptide identification through LC/MS-MS. To identify active kinases potently inhibited by dasatinib in each cell line, the active kinase of dasatinib-treated cells was compared to that of vehicle control. **C**, heat map of kinases enriched in the active kinase of dasatinib-treated cells compared to vehicle control cells (\log_2 ratio is shown). Kinases that are active at baseline, inhibited >75% by dasatinib, and are common to both IDHm ICC are in blue.

quantification of the targets of dasatinib by failure of the MIB column to capture kinases bound by dasatinib. After elution, kinases are identified by mass spectroscopy (MS; Fig. 3B). To characterize on-target effects in the active kinase, IDHm or WT ICC cells were treated with dasatinib or DMSO control for 1 hour, and the relative abundance of each active kinase was quantified by MIB followed by MS. We identified six kinases that were active at baseline and inhibited 75% or more in both IDHm ICC lines treated with dasatinib (Fig. 3C; Supplementary Table S4). All of these kinases—SRC, YES1, LYN, DDR1, ABL1, and ABL2—are known targets of dasatinib with IC₅₀ values < 1 nmol/L in cell-free assays (26).

To identify key targets among those identified by the MIB method, we then turned to a genetic approach. The capacity of dasatinib to inhibit its targets is in part due to the insertion of the inhibitor in a hydrophobic pocket at the back of the ATP binding site. A threonine residue that allows access to this pocket has been designated as a "gatekeeper" (34) whose mutation to a more bulky residue, such as isoleucine, leads to loss of inhibitor binding without affecting normal kinase activity (35). We therefore used CRISPR/Cas9 technology (36, 37) to screen for gatekeeper mutations that could rescue IDHm ICC cells from dasatinib-induced cytotoxicity. SNU-1709 cells were transfected with Cas9, a guide RNA targeting the endogenous

ABL1, *ABL2*, *DDR1*, *LYN*, *YES1*, or *SRC* loci, and a donor oligonucleotide encoding the appropriate gatekeeper mutation, and subsequently treated with dasatinib for 30 days (Fig. 4A). Strikingly, the SRC gatekeeper mutation (*SRC^{T341I}*) fully rescued cell viability, resulting in the growth of dasatinib-resistant colonies, whereas none of the other guide RNAs conferred rescue (Fig. 4B). We also failed to generate viable colonies using gatekeeper mutant guides for three additional dasatinib targets, *FRK*, *CSK*, and *EPHA4* (data not shown). Thus, our data show that SRC inhibition is critical for dasatinib-mediated cytotoxicity in IDHm ICC, although we cannot rule out additional targets that may contribute to this effect.

We confirmed that SNU-1079-*SRC^{T341I}* cells were highly resistant to dasatinib-induced cytotoxicity relative to the parental line (Fig. 4C and D). Sequencing analysis demonstrated that the SNU-1079-*SRC^{T341I}* cells had the expected genomic editing of the *SRC* locus (Supplementary Fig. S5A). In addition, whereas dasatinib fully inhibited SRC activity in the parental cells, as evidenced by loss of Y416 phosphorylation, the *SRC^{T341I}* cells were resistant (Fig. 4E). Importantly, this was not unique to SNU-1079 cells, as genome editing to introduce the *SRC^{T341I}* gatekeeper mutation into a second IDHm ICC cell line, RBE, also resulted in marked resistance to dasatinib (shifting IC₅₀ >500-fold; Fig. 4F, top left panel, and Supplementary Fig. S5B). In keeping with these results, gatekeeper mutant expression rescued the effect of dasatinib on key signaling pathways, with *SRC^{T341I}* cells maintaining p-p70S6K and pS6 levels upon dasatinib treatment, in contrast to what is seen in parental cells (Fig. 4G). Confirming the specificity of the rescue, *SRC^{T341I}* cells also showed increased resistance to saracatinib and bosutinib, but not ponatinib, which is designed to overcome this gatekeeper mutation (Fig. 4F). In further validation studies, shRNA-mediated knockdown of *SRC* also reduced pS6 levels and abolished growth specifically in IDHm ICC cells (Supplementary Fig. S5C and S5D). Thus, the potent cytotoxicity of dasatinib against IDHm ICC is due to the critical requirement for SRC tyrosine kinase activity in maintaining the growth and viability of these cells.

DISCUSSION

ICC is a highly lethal malignancy with limited therapeutic options and no effective screening or prevention strategies. The discovery of frequent *IDH* mutations in ICC as well as in other cancers has led to great enthusiasm for both unraveling their unusual effects on cancer cell biology and interrogating the mutant enzymes as drug targets. The development of potent, specific, and nontoxic mutant *IDH* inhibitors and their effective deployment as single agents in IDHm leukemia represent important advances in oncology (21). Additionally, recent experimental studies have highlighted other potential synthetic lethal vulnerabilities in different IDHm cancers involving targeting the BET domain family of chromatin regulators, the *BCL2* antiapoptotic protein, and the mitochondrial NADH salvage pathway enzyme NAMPT (28, 29, 38). Early preclinical work and clinical trials data indicate that mutant *IDH* inhibition may provide benefit in solid tumors, although the effects appear more modest than those seen in leukemia (22). Likewise, we did not observe outlier sensitivity in our human IDHm ICC cell lines to inhibitors

of *BCL2*, NAMPT, or BET proteins (Supplementary Fig. S3D and S3E and data not shown), suggesting that such vulnerabilities may be both genotype- and cancer-specific.

Our studies were centered on utilizing an unbiased approach to identify FDA-approved or advanced clinical compounds that are effective against IDHm ICC. In addition to their therapeutic potential, these drugs can serve as functional probes to expose critical growth and survival pathways. However, the identification of the specific targets involved in the biological response to these compounds is often a significant challenge. In the case of promiscuous multi-kinase inhibitors, such as dasatinib, it can be particularly difficult to establish key targets mediating cytotoxicity when specific kinase driver mutations are absent. To address this, we used a comprehensive approach, using an MIB column strategy to generate an unbiased list of likely targets, combined with CRISPR/Cas9-mediated genome editing to render the endogenous kinases resistant to dasatinib binding. These studies revealed that IDHm ICCs have a pronounced and unexpected dependency on SRC signaling for cell growth and survival. We show that IDHm ICCs are profound outliers in their responsiveness to dasatinib, and that SRC gatekeeper mutants confer almost complete protection of these cells. Notably, although it is recognized as the first known oncogene, there are surprisingly few examples of human cancers where endogenous SRC has been established to be critical for survival (39). These findings suggest a clinical path forward for the use of dasatinib or other SRC inhibitors in the treatment of IDHm ICC. Moreover, the methods used here provide a framework for the systematic identification of critical targets of kinase inhibitors in sensitive cancer cell lines.

Understanding the basis of the specific dasatinib hypersensitivity of IDHm ICC remains an important outstanding question. This effect does not appear to be associated with differences in overall SRC activity, because levels of SRC expression and activity did not correlate with dasatinib sensitivity or *IDH* status. In particular, SRC kinase activity was comparable in *IDH* WT and mutant cell lines (data not shown), and *IDH* WT and mutant ICCs in The Cancer Genome Atlas database show similar *SRC* mRNA levels (data not shown). Nevertheless, there are marked distinctions in the downstream pathways controlled by SRC between IDHm and WT ICC (Fig. 3A; Supplementary Fig. S5C). It is noteworthy that all IDHm ICC models evaluated, including both human and murine cells harboring either *IDH1* or *IDH2* mutations, demonstrated a similar level of sensitivity to dasatinib. Yet, expression of mutant *IDH* alone is not sufficient to confer this response, as IDHm cells from other solid tumors (lung cancer and chondrosarcoma) had 5- to 100-fold higher IC₅₀ than IDHm ICC (Supplementary Fig. S3C). Moreover, ectopic expression of mutant *IDH* only marginally increased the sensitivity of WT ICC cells (Supplementary Fig. S6A–C). Thus, *IDH* mutations confer dasatinib hypersensitivity when present during ICC pathogenesis, but not when expressed exogenously in established tumors, which may reflect the unique selective pressures induced by these mutations or the 2-HG oncometabolite during tumorigenesis. Accordingly, ICC tumors harboring endogenous *IDH* mutations define a distinct subtype of ICC, with a characteristic transcriptional and epigenetic profile (18, 20).

RESEARCH BRIEF

Saha et al.

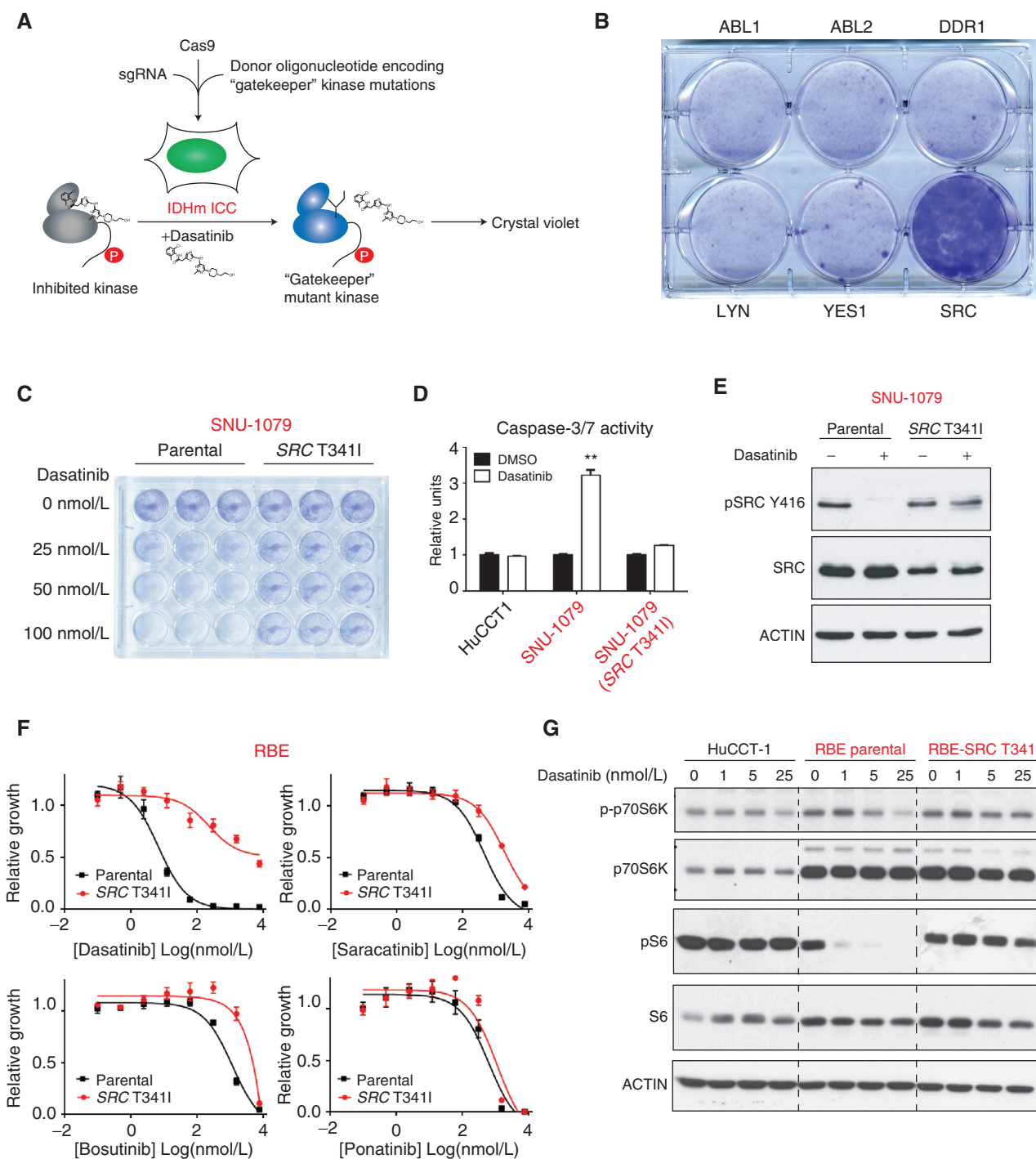


Figure 4. SRC is a critical dasatinib target in IDHm ICC. **A**, schematic for the introduction of "gatekeeper" mutants into the endogenous loci encoding dasatinib targets in IDHm ICC cells. Plasmids containing Cas9 and a single-guide RNA (sgRNA) targeting each individual kinase were cotransfected with a donor oligonucleotide encoding the gatekeeper mutation for each kinase. The gatekeeper mutation prevents the endogenously expressed kinase from binding to and being inhibited by dasatinib, thus allowing dasatinib targets to remain active. Cells were then plated at confluence and treated with dasatinib 50 nmol/L for 30 days in a 6-well plate. **B**, crystal violet staining of viable cells treated as in **A**, demonstrating that introduction of the SRC T341I gatekeeper mutation rescues SNU-1079 cells from dasatinib-induced cytotoxicity. **C**, crystal violet stain of SNU-1079 parental cells and cells harboring an endogenous SRC T341I mutation following treatment with increasing doses of dasatinib or DMSO control (0 nmol/L) for 24 hours. **D**, caspase-3/7 activity of HuCCT1 cells, SNU-1079 parental cells, and SNU-1079 SRC T341I cells treated with dasatinib 100 nmol/L for 24 hours relative to DMSO control. **, $P < 0.01$. **E**, dasatinib treatment (50 nmol/L) for 2 hours causes loss of pSRC (Tyr416) in parental SNU-1079 cells but not in SNU-1079 SRC T341I cells, as shown by immunoblot of insoluble fractions. **F**, proliferation curves of RBE parental (black) or SRC T341I (red) treated with increasing doses of dasatinib, saracatinib, bosutinib, and ponatinib. **G**, immunoblot of lysates from RBE parental and SRC T341I cells showing that the SRC gatekeeper mutation rescues p-p70 S6 kinase (Thr389) and pS6 (Ser235/236) levels in dasatinib-treated cells.

Rigorous preclinical and clinical studies will be required to determine the optimal strategy to exploit SRC inhibition in patients with IDHm ICC. As there is currently no standard second-line therapy, we have initiated a clinical trial to investigate the safety and efficacy of dasatinib in patients with IDHm ICC who have progressed on chemotherapy. In addition, dasatinib could be used as an “anchor” for exploring combinatorial strategies in IDHm ICC. The possible synergy of dasatinib with mutant IDH inhibitors, for instance, remains an active area of investigation. Unfortunately, our preliminary studies suggest that this combination may be antagonistic in some tumors, which implies a potential role for 2-HG or mutant IDH enzymatic activity in maintaining dasatinib hypersensitivity (data not shown). Thus, an unbiased approach utilizing high-throughput combination drug screens may be needed to identify agents that synergize with dasatinib to further inhibit growth or enhance cell death in IDHm ICC.

Beyond targeting SRC in IDHm ICC, our approach provides a proof of principle for the use of high-throughput drug screening to identify novel drug efficacies in molecular subsets of BTC. In this regard, recent genetic studies have revealed a remarkable genetic heterogeneity in these diseases, with numerous recurrent mutations in epigenetic modifiers, receptor tyrosine kinases, and tumor suppressor pathways (7–14). Here, we provide a database of the relative sensitivities of 17 BTC cell lines to 122 approved or advanced clinical compounds as a resource (Supplementary Table S1), which may be used as a basis for additional translational studies linking genomic biomarkers to drug sensitivities.

METHODS

Cell Lines

Cell lines were obtained from the following sources: DSMZ (EGI-1), Riken Bioresource Center (HuCCT1, G-415, RBE, SSP-25, TFK-1, TGBC14TKB, YSCCC, TKKK, HuH-28), Korean Cell Line Bank (SNU-245, SNU-308, SNU-478, SNU-869, SNU-1079, SNU-1196), ATCC (HT-1080, SW-1353), and ECACC (COR-L105). CC-LP-1 and CC-SW-1 were kind gifts from Dr. P.J. Bosma (Academic Medical Center, Amsterdam, the Netherlands), SG231 from Dr. A.J. Demetris (University of Pittsburgh, Pittsburgh, PA), MMNK-1 from Dr. J. Luyendyk (University of Kansas Medical Center, Kansas City, KS), and HKGZ-CC from Drs. X.Y. Guan and S. Ma (The University of Hong Kong, Hong Kong, P.R. China). All cell lines were authenticated by short tandem repeat (STR) DNA profiling the cell line bank from which they were obtained. Otherwise, CC-LP-1, CC-SW-1, SG231, HKGZ-CC, MMNK-1, ICC1, ICC2, and ICC5 were authenticated by STR DNA profiling through ATCC between December 2015 and March 2016. Additional information regarding culture conditions for all BTC cell lines is described in Supplementary Table S5. Information about cell lines used in the large cell line screen of dasatinib and saracatinib can be found in the High-Throughput Drug Screen section. Cell lines were grown at 37°C under 5% CO₂ in their required growth medium (Gibco) supplemented with 10% fetal bovine serum and 1% penicillin and streptomycin. To establish murine and human ICC cell lines, freshly isolated tumor specimens from *Kras*^{G12D}; *IDH2*^{R172K} (SS49; ref. 20) or *Kras*^{G12D}; *Trp53*^{f/f} (537 and 425; ref. 30) mice or ICC resection specimens, per our Institutional Review Board (IRB)-approved protocol (DFCI, #13-162), were minced with sterile razor blades, digested with trypsin for 30 minutes at 37°C, and then resuspended in RPMI supplemented with 10% fetal bovine serum and 1% penicillin/streptomycin (Gibco, #15140-

122) for murine lines or RPMI supplemented with 20% fetal bovine serum, 1% L-glutamine (Gibco, #25030-081), 1% MEM Non-Essential Amino Acids Solution (Gibco, #11140-050), 1% Sodium Pyruvate (Gibco, #11360-070), 0.5% penicillin/streptomycin, 10 µg/mL gentamicin (Gibco, #15710-064), and 0.2 Units/mL human recombinant insulin (Gibco, #12585-014) for human lines and seeded on plates coated with rat tail collagen (BD Biosciences). Cells were passaged by trypsinization, adapted to RPMI supplemented with 10% fetal bovine serum and 1% penicillin/streptomycin (human lines) and transferred to uncoated tissue-culture plates prior to proliferation assays. All studies were done on cells cultivated for fewer than ten passages.

Mice and Xenograft Experiments

Mice were housed in pathogen-free animal facilities. All experiments were conducted under protocol 2005N000148 approved by the Subcommittee on Research Animal Care at Massachusetts General Hospital. For murine SS49 xenografts, 1 × 10⁵ cells were injected subcutaneously into the flanks of 6-to-8-week-old female CB17/*lcr-Prkdc*^{scid}/*lcrCr* mice (561; Charles River). When tumors reached ~125 mm³, mice were treated with either vehicle control or dasatinib 50 mg/kg daily by oral gavage. Tumor size was measured daily with a digital caliper. To develop an IDHm human PDX, we obtained tissue from a fresh resection specimen from a patient with an *IDH1* R132C mutant ICC tumor, per our IRB-approved protocol (DFCI, #13-162). The tissue was rinsed in Hank's Balanced Salt Solution and cut into 0.3–0.5-mm³ pieces with sterile razor blades. These tumor pieces were implanted subcutaneously into 6-to-8-week-old female NSG mice (NOD.Cg-*Prkdc*^{scid} *Il2rg*^{tm1Wjl}/*SzJ*, 00557; The Jackson Laboratory). Upon reaching ~900 mm³, mice were randomized to either vehicle control or dasatinib 50 mg/kg daily by oral gavage for 7 days prior to harvest.

High-Throughput Drug Screen

High-throughput drug screening and sensitivity modeling (curve fitting and IC₅₀ estimation) was performed essentially as described previously (40). All cell lines were sourced from commercial vendors except as indicated. Cells were grown in RPMI or DMEM/F12 medium supplemented with 5% FBS and penicillin/streptomycin, and maintained at 37°C in a humidified atmosphere at 5% CO₂. Cell lines were propagated in these two media in order to minimize the potential effect of varying the media on sensitivity to therapeutic compounds in our assay, and to facilitate high-throughput screening. To exclude cross-contaminated or synonymous lines, a panel of 92 SNPs was profiled for each cell line (Sequenom) and a pair-wise comparison score was calculated. In addition, STR analysis (AmpFLSTR Identifiler; Applied Biosystems) was performed and matched to an existing STR profile generated by the providing repository. More information on the cell lines screened, including their SNP and STR profiles, is available on the Genomics of Drug Sensitivity in Cancer project website (41). All drugs were sourced from Selleck Chemicals or provided by the laboratory of Nathanael Gray (Harvard Medical School) after stringent quality control. This screen did not include AGI-5027 or other mutant IDH inhibitors. Briefly, cells were seeded at variable density to ensure optimal proliferation during the assay. Drugs were added to the cells the day after seeding in a 9-dose series with doses 2-fold apart covering a range of 256-fold. Concentrations were chosen as possible based on known in cell targeting to minimize off-target effects. Viability was determined using either Syto60 or resazurin after 3 days of drug exposure as previously described (34). Figures 1B–C displaying drug response across the ICC lines were prepared using GENE-E (42).

Proliferation Assays

Cells were plated in 96-well plates (1,000 cells/well) in culture medium. The following day, increasing doses of either AGI-5027

(ML309, a gift from Agios Pharmaceuticals; ref. 43), dasatinib (S1021; Selleck Chemicals), saracatinib (S1006; Selleck Chemicals), bosutinib (S1014; Selleck Chemicals), ponatinib (S1490; Selleck Chemicals), Torin 1 (S2827; Selleck Chemicals), FK866 (S2799; Selleck Chemicals) or DMSO control (BP231-100; Fisher Scientific) were added, and the cells were allowed to grow until DMSO-treated wells reached confluence (5–7 days). To quantify viable cells, MTT (M-6494; ThermoFisher Scientific) was added to the culture media at a final concentration of 1 mg/mL and incubated for 3 hours at 37°C. Formazan crystals were solubilized with 100 µL/well of DMSO and absorbance was read at 490 nm and normalized to DMSO control. MTT proliferation assays were performed in duplicate, and data are represented as mean ± SEM among three independent experiments unless otherwise indicated in the figure legend.

Constructs and Viral Infection

Human *IDH1*^{R132C}, *IDH2*^{R172K}, and pMSCV-blast constructs were described previously (20). The following lentiviral plasmids were used: Human shSRC #1 (TRCN0000195339) target sequence: 5'-CATC CTCAGGAACCAACAATT-3'; shSRC #2 (TRCN0000199186) target sequence: 5'-CTGACTGAGCTACCACAAAG-3'; shSRC #3 (TRC N0000038150) target sequence: 5'-GACAGACCTGTCCTTCAA GAA-3'. pLKO.1 shRNA with target sequence 5'-GCAAGCTGACC CTGAAGTTCAT-3' was used as a negative control. Viral particles containing the above-mentioned plasmids were synthesized using either lentiviral (pCMV-dR8.91) or retroviral (pCL-ECO) packaging plasmids with pCMV-VSV-G (Addgene). Cells were infected by incubating with virus and 8 µg/mL polybrene (Millipore, #TR-1003-G). Twenty-four hours later, cells were selected in 2.5 µg/mL puromycin for at least 2 days, and the pooled populations were used for various experiments.

Immunoblot Analysis

Cell extracts were prepared in 1× RIPA buffer (150 mmol/L NaCl, 1% IGEPAL, 0.1% SDS, 50 mmol/L Tris, 0.5% DOC) supplemented with a protease inhibitor cocktail (Complete; Roche Applied Science) and phosphatase inhibitors (Phosphatase Inhibitor Cocktail Sets I and II; Calbiochem) and quantified by BCA Protein Assay (Thermo Scientific). For detection of pSRC Y416, cells were first fractionated using a NE-PER Extraction Kit (7833; Thermo Scientific experiments) per the manufacturer's recommended protocol, and the insoluble fraction is shown. Protein (30 µg) was resolved on 8% to 11% SDS-PAGE gels and transferred onto PVDF membranes (GE Healthcare Life Sciences). Membranes were blocked in TBS with 5% nonfat milk and 0.1% Tween 20 (BP 337-500; Fisher Scientific) and probed with antibodies against IDH1 (#3997S; Cell Signaling Technology), IDH2 (NBP2-22166; Novus Biologicals), p-p70S6 kinase (Thr389; #9234; Cell Signaling Technology), total p70S6K (#2708; Cell Signaling Technology), pS6 (Ser235/236) (#4858; Cell Signaling Technology), total S6 (#2217; Cell Signaling Technology), pERK1/2 (Thr202/Tyr204) (#9101; Cell Signaling Technology), total ERK1/2 (#4695; Cell Signaling Technology), pSTAT3 (Ser727) (#9134; Cell Signaling Technology), total STAT3 (#9139; Cell Signaling Technology), BCL2 (#2872; Cell Signaling Technology), MCL1 (sc-819; Santa Cruz Biotechnology), pSRC Y416 (#6943; Cell Signaling Technology), total SRC (#2123; Cell Signaling Technology), or ACTIN (A5316; Sigma-Aldrich) as a loading control. Bound proteins were detected with horseradish peroxidase-conjugated secondary antibodies (Vector Biolaboratories) and SuperSignal West Pico Luminol/Enhancer Solution (Thermo Scientific). All primary antibodies were used at 1:1,000 dilution except for those against IDH2 (1:500), MCL1 (1:200), pS6 (1:2,000), and ACTIN (1:10,000).

Multiplex Inhibitor Bead Column

Kinase chromatography and mass spectrometry were performed as described previously (33). Briefly, compounds were commercially

obtained or synthesized directly, and then affixed to sepharose using 1-Ethyl-3-(3-dimethylaminopropyl)carbodiimide-catalyzed peptide coupling chemistry. Cell lysates were then diluted in binding buffer with 1 mol/L NaCl, and affinity purification was performed with gravity chromatography. The bound kinases were stringently washed and then eluted with hot SDS before extraction and tryptic digest. Liquid chromatography-tandem mass spectrometry (LC/MS-MS) was performed on a Velos Orbitrap (Thermo Scientific) with in-line high-performance liquid chromatography (HPLC) using an EASY-spray column (Thermo Scientific). Label-free quantification was performed with Skyline (44), and statistical analysis with Ms Stats (45).

Caspase-3/7 Activity

Cells were plated at confluence (10,000 cells/well) and allowed to adhere for 24 hours in 96-well plates. The following day, the cells were treated with dasatinib 100 nmol/L. After incubation with dasatinib for 24 hours, caspase-3/7 activity was assessed using a Caspase-Glo 3/7 Assay (G8090; Promega) as per the manufacturer's recommended protocol. Data are represented as mean ± SD between technical triplicates (Fig. 2C) or duplicates (Fig. 4D).

Crystal Violet Staining

Cells were plated at confluence in 24-well plates (100,000 cells/well) and allowed to adhere overnight. The following day, the cells were treated with DMSO or dasatinib 100 nmol/L. Twenty-four hours later, the media were aspirated and cells were washed with PBS, prior to fixation with ice-cold methanol for 20 minutes. The cells were then stained with 0.5% crystal violet in 25% methanol for 20 minutes at room temperature. Next, crystal violet stain was aspirated and cells were rinsed in tap water until excess crystal violet stain was removed (~20 minutes).

CRISPR/Cas9-Mediated Genome Editing

Plasmids used in this study can be found in Supplementary Table S6, and the sequences of oligonucleotides can be found in Supplementary Table S7. Target kinase loci in RBE and SNU-1079 cells were sequenced to identify and account for any cell-type-specific polymorphisms. To do so, the genomic sequence flanking the intended genome-editing alteration was amplified using Phusion Hot Start Flex DNA Polymerase (New England Biolabs) with the primers listed in Supplementary Table S7. The resulting PCR amplicons were cloned using the Zero Blunt TOPO PCR Cloning Kit (Invitrogen), transformed into *E. coli* XL-1 blue competent cells, and ~20 to 25 colonies were grown overnight at 37°C in TB media prior to miniprep (MGH DNA Core) and Sanger sequencing. Single-guide RNAs (sgRNA) targeting the putative locations of kinase gatekeeper mutations were designed so that the SpCas9 binding site overlapped the desired change. Oligonucleotides corresponding to the spacer sequence of the target site (Supplementary Table S7) were annealed and ligated into BsmBI cut BPK1520 (46) to generate the final sgRNA plasmids. Donor oligonucleotides were designed to include the desired gatekeeper mutation, as well as nonsynonymous changes to prevent re cleavage of the corrected allele (Supplementary Table S7). Transfection conditions for both RBE and SNU-1079 cells were first optimized with the Cell Line Optimization Nucleofector Kit for Nucleofector Device (Lonza) and a Nucleofector 2b Device (Lonza) according to the manufacturer's recommended protocol. Using the Cell Line Nucleofector Kit L (VVCA-1005; Lonza) and program A-020, 1.5 µg of Cas9 expression plasmid that encoded either WT SpCas9 (JDS246; ref. 47) or SpCas9-VQR (MSP469; ref. 46), 500 ng of sgRNA expression plasmid (Supplementary Table S6), and 150 pmol of donor oligonucleotide (Supplementary Table S7) were transfected for each individual kinase into 1 × 10⁶ RBE or 2.5 × 10⁶ SNU-1079 cells. Following transfection, the cells were split into three separate wells on 6-well plates. Genome editing was allowed to proceed for

3 days, prior to treating the cells with dasatinib 50 nmol/L for 30 days to select for dasatinib-resistant cells. Crystal violet staining of one of the three wells is shown in Fig. 4B, and the second and third wells were used for confirmation of the appropriate SRC mutation and subsequent assays. Successful insertion of gatekeeper mutations in the endogenous *ABL1*, *ABL2*, *DDR1*, *LYN*, and *YES1* loci was not confirmed, as no viable colonies survived dasatinib selection. Control transfections without the donor oligonucleotide containing the gatekeeper mutation were performed in parallel and did not yield any resistant colonies for any of the kinases attempted (data not shown).

Histology and Immunohistochemistry

Tissue samples were fixed overnight in 4% buffered formaldehyde, and then embedded in paraffin and sectioned (5-μm thickness) by the DF/HCC Research Pathology Core. Hematoxylin and eosin staining was performed using standard methods. For immunohistochemistry, unstained slides were baked at 55°C overnight, deparaffinized in xylenes (2 treatments, 6 minutes each), rehydrated sequentially in ethanol (5 minutes in 100%, 3 minutes in 95%, 3 minutes in 75%, and 3 minutes in 40%), and washed for 5 minutes in 0.3% Triton X-100/PBS (PBST) and 3 minutes in water. For antigen unmasking, specimens were cooked in a 2100 Antigen Retriever (Aptum Biologics Ltd.) in 1X Antigen Unmasking Solution, Citric Acid Based (H-3300; Vector Laboratories), rinsed 3 times with PBST, incubated for 10 minutes with 1% H₂O₂ at room temperature to block endogenous peroxidase activity, washed 3 times with PBST, and blocked with 5% goat serum in PBST for 1 hour. Anti-cleaved caspase-3 (#9661; Cell Signaling Technology) was diluted in blocking solution at a ratio of 1:300 and incubated with the tissue sections at 4°C overnight. Specimens were then washed 3 times for 3 minutes each in PBST and incubated with biotinylated secondary antibody (Vector Laboratories) in blocking solution for 1 hour at room temperature. Then, specimens were washed 3 times in PBST and treated with ABC reagent (Vectastain ABC Kit, #PK-6100) for 30 minutes, followed by three washes for 3 minutes each. Finally, slides were stained for peroxidase for 3 minutes with the DAB substrate kit (SK-4100; Vector Laboratories), washed with water, and counterstained with hematoxylin. Stained slides were photographed with an Olympus DP72 microscope. Quantification of the percentage of necrosis in tumor slides was performed by a pathologist (Y. Kato) who was blinded to the origin of the tissue. Data are represented as mean ± SEM.

2-HG Measurements

Cells were seeded in 10-cm plates and grown to ~70% confluence. Media were then refreshed 3 hours prior to harvest. To extract intracellular metabolites, cells were briefly washed with ice-cold 0.9% sodium chloride, immediately fixed with chilled acetonitrile/methanol/water (40/40/20), and frozen in liquid nitrogen. Cells were then scraped, transferred into 1.5-mL eppendorf tubes, and vortexed. A series of 3 freeze/thaw cycles on dry ice were performed. The cellular lysate was clarified by centrifugation at 15,000 × g at 4°C for 15 minutes. Clarified lysate was then directly analyzed by HPLC-MS as described previously (48).

Statistical Analysis

For studies following the high-throughput screen, GI₅₀ (defined as the concentration required to inhibit cell proliferation to 50% of untreated control) determinations were made with GraphPad Prism software. A two-tailed Student *t* test was used to assess significance for Caspase-3/7 activity assays, histologic analysis of the percentage of tumor necrosis and the effect of SRC knockdown on proliferation. Analysis of variance (ANOVA) was used to analyze significance for the effect of dasatinib on SS49 xenograft growth. *P* values <0.05 were considered statistically significant.

Disclosure of Potential Conflicts of Interest

M.J. Garnett reports receiving commercial research support from AstraZeneca. J.K. Joung reports receiving a commercial research grant from AstraZeneca; has ownership interest (including patents) in Editas Medicine, Transposagen, and Poseida Therapeutics; and is a consultant/advisory board member for Editas Medicine, Horizon Discovery, and Transposagen. C.H. Benes reports receiving commercial research grants from Amgen and Novartis. No potential conflicts of interest were disclosed by the other authors.

Authors' Contributions

Conception and design: S.K. Saha, J.D. Gordan, M.S. Najem, A.X. Zhu, C.H. Benes, N. Bardeesy

Development of methodology: S.K. Saha, B.P. Kleinstiver, M.S. Najem, L. Shi, U. McDermott, Y. Mizukami, J.K. Joung, K.M. Shokat, C.H. Benes, N. Bardeesy

Acquisition of data (provided animals, acquired and managed patients, provided facilities, etc.): S.K. Saha, J.D. Gordan, P. Vu, J.-C. Yeo, L. Shi, Y. Kato, R.S. Levin, L.J. Damon, R.K. Egan, M.J. Garnett, R.L. Jenkins, K.M. Rieger-Christ, T.B. Sullivan, A.S. Liss, L. Goyal, A.X. Zhu, C.H. Benes, N. Bardeesy

Analysis and interpretation of data (e.g., statistical analysis, biostatistics, computational analysis): S.K. Saha, J.D. Gordan, M.S. Najem, L. Shi, Y. Kato, J.T. Webber, A.X. Zhu, C.H. Benes, N. Bardeesy

Writing, review, and/or revision of the manuscript: S.K. Saha, J.D. Gordan, B.P. Kleinstiver, L. Shi, K.M. Rieger-Christ, A.S. Liss, L. Goyal, C.R. Ferrone, A.X. Zhu, C.H. Benes, N. Bardeesy

Administrative, technical, or material support (i.e., reporting or organizing data, constructing databases): S.K. Saha, P. Greninger, A.F. Hezel, Y. Mizukami, A.X. Zhu, N. Bardeesy

Study supervision: S.K. Saha, J.K. Joung, C.H. Benes, N. Bardeesy

Acknowledgments

The authors thank Nathanael Gray of Harvard Medical School for providing screening compounds, and members of the Bardeesy and Benes labs for helpful discussions.

Grant Support

This work was supported by a Translational Research Award from the V Foundation to N. Bardeesy, C.H. Benes, and A.X. Zhu, and by a grant from TargetCancer Foundation to N. Bardeesy. N. Bardeesy is the holder of the Gallagher Chair in Gastrointestinal Cancer Research at Massachusetts General Hospital. S.K. Saha is supported by an NCI-Mentored Clinical Scientist Research Career Development Award (1K08CA194268-01). N. Bardeesy and S.K. Saha are supported by the DF/HCC GI SPORE (P50CA127003). J.D. Gordan was supported by an American Cancer Society Postdoctoral Grant. K.M. Shokat is a Howard Hughes Medical Institute Investigator. B.P. Kleinstiver was supported by a Natural Sciences and Engineering Research Council of Canada Postdoctoral Fellowship. C.H. Benes, U. McDermott, and M.J. Garnett are supported by a grant from the Wellcome Trust (102696). J.K. Joung is supported by an NIH Director's Pioneer Award (DP1 GM105378) and is a consultant for Horizon Discovery. J.K. Joung has financial interests in Editas Medicine, Hera Testing Laboratories, Poseida Therapeutics, and Transposagen Biopharmaceuticals. J.K. Joung's interests were reviewed and are managed by Massachusetts General Hospital and Partners HealthCare in accordance with their conflict of interest policies.

The costs of publication of this article were defrayed in part by the payment of page charges. This article must therefore be hereby marked *advertisement* in accordance with 18 U.S.C. Section 1734 solely to indicate this fact.

Received December 8, 2015; revised May 13, 2016; accepted May 16, 2016; published OnlineFirst May 26, 2016.

REFERENCES

- Razumilava N, Gores GJ. Cholangiocarcinoma. *Lancet* 2014;383:2168–79.
- Khan SA, Thomas HC, Davidson BR, Taylor-Robinson SD. Cholangiocarcinoma. *Lancet* 2005;366:1303–14.
- Saha SK, Zhu AX, Fuchs CS, Brooks GA. Forty-year trends in cholangiocarcinoma incidence in the U.S.: intrahepatic disease on the rise. *Oncologist* 2016;21:594–9.
- Hainsworth JD, Rubin MS, Spigel DR, Boccia RV, Raby S, Quinn R, et al. Molecular gene expression profiling to predict the tissue of origin and direct site-specific therapy in patients with carcinoma of unknown primary site: a prospective trial of the Sarah Cannon research institute. *J Clin Oncol* 2013;31:217–23.
- Varadharaj GR, Raber MN. Cancer of unknown primary site. *N Engl J Med* 2014;371:757–65.
- Valle J, Wasan H, Palmer DH, Cunningham D, Anthony A, Maravillas A, et al. Cisplatin plus gemcitabine versus gemcitabine for biliary tract cancer. *N Engl J Med* 2010;362:1273–81.
- Borger DR, Tanabe KK, Fan KC, Lopez HU, Fantin VR, Straley KS, et al. Frequent mutation of isocitrate dehydrogenase (IDH)1 and IDH2 in cholangiocarcinoma identified through broad-based tumor genotyping. *Oncologist* 2012;17:72–9.
- Chan-On W, Nairismagi ML, Ong CK, Lim WK, Dima S, Pairojkul C, et al. Exome sequencing identifies distinct mutational patterns in liver fluke-related and non-infection-related bile duct cancers. *Nat Genet* 2013;45:1474–8.
- Jiao Y, Pawlik TM, Anders RA, Selaru FM, Streppel MM, Lucas DJ, et al. Exome sequencing identifies frequent inactivating mutations in BAP1, ARID1A and PBRM1 in intrahepatic cholangiocarcinomas. *Nat Genet* 2013;45:1470–3.
- Kipp BR, Voss JS, Kerr SE, Barr Fletcher EG, Graham RP, Zhang L, et al. Isocitrate dehydrogenase 1 and 2 mutations in cholangiocarcinoma. *Human Pathol* 2012;43:1552–8.
- Ross JS, Wang K, Gay L, Al-Rohil R, Rand JV, Jones DM, et al. New routes to targeted therapy of intrahepatic cholangiocarcinomas revealed by next-generation sequencing. *Oncologist* 2014;19:235–42.
- Sia D, Losic B, Moeini A, Cabellos L, Hao K, Revill K, et al. Massive parallel sequencing uncovers actionable FGFR2-PPHLN1 fusion and ARAF mutations in intrahepatic cholangiocarcinoma. *Nat Commun* 2015;6:6087.
- Voss JS, Holtegaard LM, Kerr SE, Fletcher EG, Roberts LR, Gores GJ, et al. Molecular profiling of cholangiocarcinoma shows potential for targeted therapy treatment decisions. *Hum Pathol* 2013;44:1216–22.
- Wang P, Dong Q, Zhang C, Kuan PF, Liu Y, Jeck WR, et al. Mutations in isocitrate dehydrogenase 1 and 2 occur frequently in intrahepatic cholangiocarcinomas and share hypermethylation targets with glioblastomas. *Oncogene* 2012;32:3091–100.
- Cairns RA, Mak TW. Oncogenic isocitrate dehydrogenase mutations: mechanisms, models, and clinical opportunities. *Cancer Discov* 2013;3:730–41.
- Lu C, Ward PS, Kapoor GS, Rohle D, Turcan S, Abdel-Wahab O, et al. IDH mutation impairs histone demethylation and results in a block to cell differentiation. *Nature* 2012;483:474–8.
- Turcan S, Rohle D, Goenka A, Walsh LA, Fang F, Yilmaz E, et al. IDH1 mutation is sufficient to establish the glioma hypermethylator phenotype. *Nature* 2012;483:479–83.
- Wang P, Dong Q, Zhang C, Kuan PF, Liu Y, Jeck WR, et al. Mutations in isocitrate dehydrogenase 1 and 2 occur frequently in intrahepatic cholangiocarcinomas and share hypermethylation targets with glioblastomas. *Oncogene* 2013;32:3091–100.
- Saha SK, Parachoniak CA, Bardeesy N. IDH mutations in liver cell plasticity and biliary cancer. *Cell Cycle* 2014;13:3176–82.
- Saha SK, Parachoniak CA, Ghanta KS, Fitamant J, Ross KN, Najem MS, et al. Mutant IDH inhibits HNF-4alpha to block hepatocyte differentiation and promote biliary cancer. *Nature* 2014;513:110–4.
- Stein E, Tallman M, Polleyea DA, Flinn IW, Fathi AT, Stone RM, et al. Abstract CT103: Clinical safety and activity in a phase I trial of AG-221, a first in class, potent inhibitor of the IDH2-mutant protein, in patients with IDH2 mutant positive advanced hematologic malignancies. *Cancer Res* 2014;74:CT103–CT103.
- Burrus H, Mellinghoff I, Maher E, Wen P, Beeram M, Touat M, et al. Abstract PL04–05: The first reported results of AG-120, a first-in-class, potent inhibitor of the IDH1 mutant protein, in a Phase I study of patients with advanced IDH1-mutant solid tumors, including gliomas. *Molecular Cancer Therap* 2015;14:PL04–05.
- Luo J, Solimini NL, Elledge SJ. Principles of cancer therapy: oncogene and non-oncogene addiction. *Cell* 2009;136:823–37.
- Shah NP, Kasap C, Weier C, Balbas M, Nicoll JM, Bleickardt E, et al. Transient potent BCR-ABL inhibition is sufficient to commit chronic myeloid leukemia cells irreversibly to apoptosis. *Cancer Cell* 2008;14:485–93.
- Shah NP, Kim DW, Kantarjian H, Rousselot P, Llacer PE, Enrico A, et al. Potent, transient inhibition of BCR-ABL with dasatinib 100 mg daily achieves rapid and durable cytogenetic responses and high transformation-free survival rates in chronic phase chronic myeloid leukemia patients with resistance, suboptimal response or intolerance to imatinib. *Haematologica* 2010;95:232–40.
- Davis MI, Hunt JP, Herrgard S, Ciceri P, Wodicka LM, Pallares G, et al. Comprehensive analysis of kinase inhibitor selectivity. *Nat Biotechnol* 2011;29:1046–51.
- Green TP, Fennell M, Whittaker R, Curwen J, Jacobs V, Allen J, et al. Preclinical anticancer activity of the potent, oral Src inhibitor AZD0530. *Mol Oncol* 2009;3:248–61.
- Chan SM, Thomas D, Corces-Zimmerman MR, Xavy S, Rastogi S, Hong WJ, et al. Isocitrate dehydrogenase 1 and 2 mutations induce BCL-2 dependence in acute myeloid leukemia. *Nat Med* 2015;21:178–84.
- Tateishi K, Wakimoto H, Iafrate AJ, Tanaka S, Loebel F, Lelic N, et al. Extreme vulnerability of IDH1 mutant cancers to NAD⁺ depletion. *Cancer Cell* 2015;28:773–84.
- O'Dell MR, Huang JL, Whitney-Miller CL, Deshpande V, Rothberg P, Grose V, et al. Kras(G12D) and p53 mutation cause primary intrahepatic cholangiocarcinoma. *Cancer Res* 2012;72:1557–67.
- Karaman MW, Herrgard S, Treiber DK, Gallant P, Atteridge CE, Campbell BT, et al. A quantitative analysis of kinase inhibitor selectivity. *Nat Biotechnol* 2008;26:127–32.
- Duncan JS, Whittle MC, Nakamura K, Abell AN, Midland AA, Zawistowski JS, et al. Dynamic reprogramming of the genome in response to targeted MEK inhibition in triple-negative breast cancer. *Cell* 2012;149:307–21.
- Sos ML, Levin RS, Gordan JD, Oses-Prieto JA, Webber JT, Salt M, et al. Oncogene mimicry as a mechanism of primary resistance to BRAF inhibitors. *Cell Rep* 2014;8:1037–48.
- Liu Y, Shah K, Yang F, Witucki L, Shokat KM. A molecular gate which controls unnatural ATP analogue recognition by the tyrosine kinase v-Src. *Bioorg Med Chem* 1998;6:1219–26.
- Daub H, Specht K, Ullrich A. Strategies to overcome resistance to targeted protein kinase inhibitors. *Nat Rev Drug Discov* 2004;3:1001–10.
- Hsu PD, Lander ES, Zhang F. Development and applications of CRISPR-Cas9 for genome engineering. *Cell* 2014;157:1262–78.
- Sander JD, Joung JK. CRISPR-Cas systems for editing, regulating and targeting genomes. *Nat Biotechnol* 2014;32:347–55.
- Chen C, Liu Y, Lu C, Cross JR, Morris JPT, Shroff AS, et al. Cancer-associated IDH2 mutants drive an acute myeloid leukemia that is susceptible to Brd4 inhibition. *Gen Develop* 2013;27:1974–85.
- Brunton VG, Frame MC. Src and focal adhesion kinase as therapeutic targets in cancer. *Curr Opin Pharmacol* 2008;8:427–32.
- Garnett MJ, Edelman EJ, Heidorn SJ, Greenman CD, Dastur A, Lau KW, et al. Systematic identification of genomic markers of drug sensitivity in cancer cells. *Nature* 2012;483:570–5.
- [41. http://www.cancerRxgene.org](http://www.cancerRxgene.org)
- [42. http://www.broadinstitute.org/cancer/software/GENE-E/](http://www.broadinstitute.org/cancer/software/GENE-E/)
- Davis MI, Gross S, Shen M, Straley KS, Pragani R, Lea WA, et al. Biochemical, cellular, and biophysical characterization of a potent inhibitor of mutant isocitrate dehydrogenase IDH1. *J Biol Chem* 2014;289:13717–25.

44. Schilling B, Rardin MJ, MacLean BX, Zawadzka AM, Frewen BE, Cusack MP, et al. Platform-independent and label-free quantitation of proteomic data using MS1 extracted ion chromatograms in skyline: application to protein acetylation and phosphorylation. *Mol Cell Proteom* 2012;11:202–14.
45. Choi M, Chang CY, Clough T, Brody D, Killeen T, MacLean B, et al. MSstats: an R package for statistical analysis of quantitative mass spectrometry-based proteomic experiments. *Bioinformatics* 2014;30:2524–6.
46. Kleinstiver BP, Prew MS, Tsai SQ, Topkar VV, Nguyen NT, Zheng Z, et al. Engineered CRISPR-Cas9 nucleases with altered PAM specificities. *Nature* 2015;523:481–5.
47. Fu Y, Foden JA, Khayter C, Maeder ML, Reyon D, Joung JK, et al. High-frequency off-target mutagenesis induced by CRISPR-Cas nucleases in human cells. *Nat Biotechnol* 2013;31:822–6.
48. Nicolay BN, Danielian PS, Kottakis F, Lapek JD Jr., Sanidas I, Miles WO, et al. Proteomic analysis of pRb loss highlights a signature of decreased mitochondrial oxidative phosphorylation. *Gen Dev* 2015;29:1875–89.

CANCER DISCOVERY

Isocitrate Dehydrogenase Mutations Confer Dasatinib Hypersensitivity and SRC Dependence in Intrahepatic Cholangiocarcinoma

Supriya K. Saha, John D. Gordan, Benjamin P. Kleinstiver, et al.

Cancer Discov 2016;6:727-739. Published OnlineFirst May 26, 2016.

Updated version Access the most recent version of this article at:
[doi:10.1158/2159-8290.CD-15-1442](https://doi.org/10.1158/2159-8290.CD-15-1442)

Supplementary Material Access the most recent supplemental material at:
<http://cancerdiscovery.aacrjournals.org/content/suppl/2016/05/27/2159-8290.CD-15-1442.DC1>

Cited articles This article cites 46 articles, 9 of which you can access for free at:
<http://cancerdiscovery.aacrjournals.org/content/6/7/727.full#ref-list-1>

Citing articles This article has been cited by 9 HighWire-hosted articles. Access the articles at:
<http://cancerdiscovery.aacrjournals.org/content/6/7/727.full#related-urls>

E-mail alerts [Sign up to receive free email-alerts](#) related to this article or journal.

Reprints and Subscriptions To order reprints of this article or to subscribe to the journal, contact the AACR Publications Department at pubs@aacr.org.

Permissions To request permission to re-use all or part of this article, use this link
<http://cancerdiscovery.aacrjournals.org/content/6/7/727>.
Click on "Request Permissions" which will take you to the Copyright Clearance Center's (CCC) Rightslink site.